Conformational Studies of Microcystin-LR Using NMR Spectroscopy and Molecular Dynamics Calculations[†,‡]

Gull-Britt Trogen,[§] Arto Annila,[∥] John Eriksson,[⊥] Maarit Kontteli,[∥] Jussi Meriluoto,[#] Ingmar Sethson,[§] Janusz Zdunek,[▽] and Ulf Edlund*[,§]

Department of Organic Chemistry, Umeå University, S-90187 Umeå, Sweden, VTT, Chemical Technology, POB 1401 FIN-02044 Espoo, Finland, Turku Centre for Biotechnology, POB 123 FIN-20521 Turku, Finland, Department of Biochemistry and Pharmacy, Åbo Akademi University, POB 66, FIN-20521 Turku, Finland, and Department of Biophysics, Arrhenius Laboratories, Stockholm University, S-10691 Stockholm, Sweden

Received October 3, 1995; Revised Manuscript Received January 10, 1996[⊗]

ABSTRACT: NMR spectroscopy in aqueous and dimethyl sulfoxide/water solutions is used to determine the three-dimensional structures of microcystin-LR, a cyclic cyanobacterial heptapeptide toxin which is a potent inhibitor of type 1 and type 2A protein phosphatases. The conformations of this toxic peptide are studied using a simulated annealing (SA) protocol followed by refined SA calculations *in vacuo* and free MD simulations in water. Only one conformational family in each solvent is found. The peptide ring has a saddle-shaped form, essentially the same in both solvents. The structural difference observed between the two solution structures is located to the part consisting of Mdha, Ala, and Leu. This peptide segment is not present in nodularin, a cyclic pentapeptide of similar toxicity. The Arg side chain is very flexible, while the side chain of Leu is well defined. The side chain of Adda, essential for toxicity, is constrained in the vicinity of the backbone ring but appears to be flexible in the more remote part.

Cyanobacteria (blue-green algae) grow world-wide in eutrophic fresh and brackish water as well as in marine environments. They frequently cause animal and human water-based toxicosis (Carmichael, 1988a; Codd et al., 1989) as they produce a number of different toxins. Several species among the cyanobacterial genera *Microcystis*, *Oscillatoria*, *Anabena*, and *Nostoc* produce certain cyclic heptapeptide hepatotoxins called microcystins (Botes et al., 1984; Meriluoto et al., 1989; Rinehart et al., 1994; Carmichael et al., 1988b). These peptides have a common invariable cyclic structure (Scheme 1) with certain variable sections. The main structural difference between different microcystins is the variation of the two L-amino acids labeled X and Z in Scheme 1. Omitted methyl substitutions of D-*erythro*-β-methylaspartic acid (Masp)[1] and *N*-methyldehydroalanine (Mdha) are also common structural modifications (Namikoshi et al., 1992). More than 40 different microcystins have been isolated and characterized (Rinehart et al., 1994). The most prevalent toxin of this type is microcystin-LR (Scheme 1),

Scheme 1

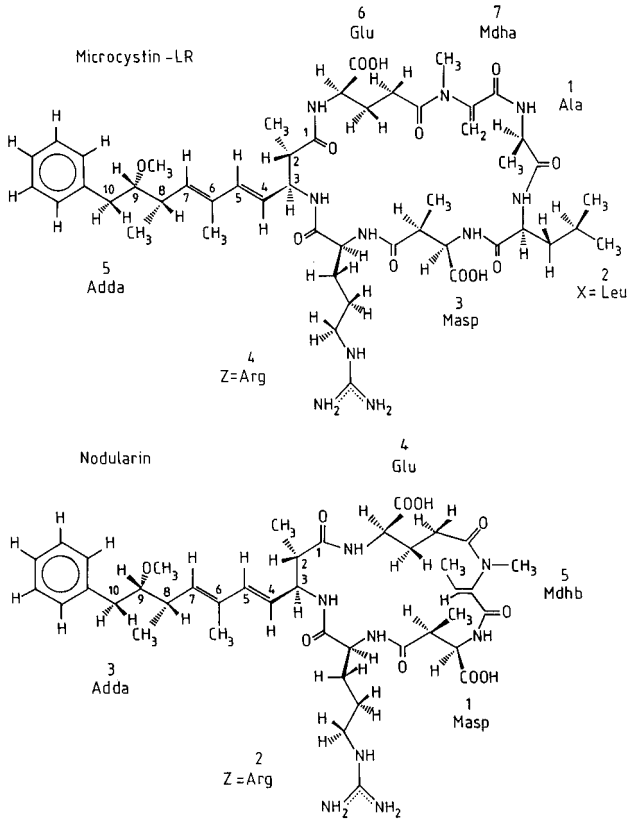

which is also the most toxic peptide known among the microcystins. A brackish water cyanobacterium, *Nodularia spumigena* (Rinehart et al., 1994; Sivonen et al., 1989), produces a related cyclic pentapeptide hepatotoxin called nodularin (Scheme 1). Both microcystins and nodularin contain the unusual amino acids (2*S*,3*S*,8*S*,9*S*)-3-amino-9-

[†] This work was supported by grants from Centre of Environmental Research (CMF) to U.E. and from the Academy of Finland and Magnus Ehrnrooth Fund to A.A.

[‡] The structure coordinates have been deposited in the Brookhaven Protein Data Bank (file name 1LCM; restraints R1LCMMR).

* To whom correspondence should be addressed.

[§] Department of Organic Chemistry, Umeå University.

[∥] VTT, Chemical Technology, Espoo.

[⊥] Turku Centre for Biotechnology, Turku.

[#] Department of Biochemistry and Pharmacy, Åbo Akademi University.

[▽] Department of Biophysics, Stockholm University.

[⊗] Abstract published in *Advance ACS Abstracts,* February 15, 1996.

[1] Abbreviations: L, leucine; R, arginine; Y, tyrosine; NMR, nuclear magnetic resonance; 2D, two dimensional; 1D, one dimensional; rmsd, root mean square deviations; MD, molecular dynamics; SA, simulated annealing; Mdha, *N*-methyldehydroalanin; Masp, D-*erythro*-β-methylaspartic acid; Adda, (2*S*,3*S*,8*S*,9*S*)-3-amino-9-methoxy-2,6,8-trimethyl-10-phenyldeca-4,6-dienoic acid; Mdhb, 2-(*N*-methylamino)-2-butenoic acid; NOE, nuclear Overhauser effect; DMSO, dimethyl sulfoxide.

methoxy-2,6,8-trimethyl-10-phenyldeca-4,6-dienoic acid (Adda) and D-*erythro*-β-methylaspartic acid (Masp). Microcystins contain a dehydroalanine moiety while nodularin has a 2-(methylamino)-2-dehydrobutyric (Mdhb) acid unit. A cyclic pentapeptide toxin designated motuporin, which is closely related structurally to nodularin, has been isolated from the marine sponge *Theonella swinhoei* (de Silva et al., 1992). The structure of motuporin is that of (L-Val^2)-nodularin—a variation of the arginine residue in nodularin which corresponds to the variation of the X,Z-amino acid residues in microcystins.

Microcystins, as well as nodularin and motuporin, are biologically and biochemically highly interesting compounds as they are potent and specific inhibitors of type-1 and type-2A protein phosphatases, two of the major serine-/threonine-specific protein phosphatases in eukaryotic cells. Their inhibitor activities are similar to those of okadaic acid and calyculin-A (Matsushima et al., 1990; Sivonen et al., 1992a; MacKintosh et al., 1990; Eriksson et al., 1990). All of these compounds have been a considerable asset in elucidating the *in vivo* functions of protein phosphatases. Interestingly, microcystins and presumably nodularin are also tumour promoters (Fujiki et al., 1991; Nishiwaki et al., 1992) with potencies equal to those of okadaic acid and calyculin-A (Fujiki et al., 1989).

The stereochemistry of the Adda residue seems to be essential for activity and toxicity of microcystins (Harada et al., 1990a; Namikoshi et al., 1990). When the configuration of the Adda double bond system is altered from (4*E*,6*E*), to (4*E*,6*Z*), the resulting stereoisomer shows no toxicity (Harada et al., 1990a,b). Hydrogenation or ozonolysis of this diene system also gives nontoxic products.[2] Some variations of the Adda structure are, however, without effects on the biological activity. The toxicity of microcystins with an acetoxy group at the Adda C-9 position is equal to that of microcystins with a methoxy group at the same position (Namikoshi et al., 1990). The amino acid Adda is itself reported to be a nontoxic component (Namikoshi et al., 1989).

While there is ample information as to the toxicity and mechanisms of action of these cyanobacterial peptides, their three-dimensional structures are only now emerging. Preliminary NMR spectroscopy studies have been performed on microcystin-LR and microcystin-LY in DMSO (Bagu et al., 1995) and on microcystin-LR and motuporin in water (Rudolpf-Böhner et al., 1994). In these studies, the various structures proposed for the peptides have been based exclusively on distance geometry calculations. The crystal structure of protein phosphatase-1, complexed with microcystin-LR, has recently been determined (Goldberg et al., 1995).

The biological relevance of the examination of peptides in DMSO been discussed (Saulitis et al., 1992). Since the receptors for these molecules most likely are composed of both lipophilic and hydrophobic portions, DMSO will presumably better mimic these properties than can aqueous solutions. Furthermore, in order to mimic the viscosity in cells, a DMSO-d_6/H_2O (80/20, v/v) cryoprotective mixture was chosen as solvent. The viscosity varies from 10 to 2 cp in the temperature range of 265−315 K vs a viscosity of 0.8 cp for water at room temperature (Shichman & Amey, 1971). At low temperature this mixture has properties close to that of water at room temperature (Motta et al., 1988; Amodeo et al., 1991).

Here we present the structures of microcystin-LR in water and in DMSO/water as obtained from restrained MD calculations *in vacuo*. In addition, the possibility of conformational exchange has been explored by *J*-coupling analysis, by amide proton exchange studies, and by unrestrained MD simulations in water. This has enabled an evaluation of whether the resultant restrained MD structures represent reasonable pictures of the solution structures or if they represent averages of substantially different conformations in rapid exchange.

Table 1: NMR Parameters

	acquisition time (s)	number of increments	mixing time (ms)	number of transients
		DMSO/H_2O		
TOCSY	0.205	512	50, 80	32
NOESY	0.205	256	80, 100, 150, 200,[a] 250	16
ROESY	0.205	256	50	32
DQF-COSY	0.819	1024		32
		H_2O/D_2O		
TOCSY	0.320	320	80, 120	32
NOESY	0.320	400	80, 160,[a] 320, 480, 640	32
ROESY	0.320	300	200	32
COSY	0.640	512		32

[a] Used for the evaluation of distance constraints.

EXPERIMENTAL PROCEDURES

Sample Preparation. Microcystin-LR was purified (Meriluoto et al., 1989) from *Microcystis aeruginosa* collected from a natural bloom in the lake Akersvatn, Norway (Berg et al., 1987). For the NMR measurements, two samples, one in DMSO-d_6/H_2O (80/20, v/v) and the other in H_2O/D_2O (94/6, v/v), were prepared from the lyophilized peptide. The DMSO/water solution contained 2−2.5 mg of freeze-dried microcystin in 0.56 mL of DMSO and 0.14 mL of 20 mM phosphate buffer giving a pH value of 5.9. The aqueous sample was prepared by dissolving 1.4−1.6 mg of material in water (including D_2O) to yield a concentration of approximately 2 mM. The pH was then adjusted to 5.6 with NaOH and HCl. Later the peptide was relyophilized and dissolved in D_2O for exchange rate measurements. The samples contained a stereoisomer of microcystin-LR as a minor component (<5%). An estimated 20 mM concentration of acetonitrile remained in the water sample as an impurity emanating from the purification medium.

NMR Experiments. The NMR spectra of the sample dissolved in DMSO/water were acquired at 500 MHz (Varian Unity 500 and Bruker AMX2 500), while the NMR spectra of the sample dissolved in water were acquired at 600 MHz (Varian Unity 600). In all experiments the solvent signal was suppressed by continuous presaturation ($\gamma\beta_1 \approx 100$ Hz) during the relaxation delay of 2−3 s. The 2D NMR spectra were acquired in a phase sensitive mode in t_1, i.e., TPPI (Bruker) or States−TPPI (Varian). Parameters for the NMR experiments are compiled in Table 1.

The NMR experiments were conducted at 4 °C in DMSO/water and at 1 °C in water. The molecular tumbling is in a

[2] A. M. Dahlem, V. R. Beasley, K.-I. Harada, K. Matsuura, M. Suzuki, C. A. Harvis, K. A. Rinehart, and W. W. Carmichael. The structure/toxicity relationships of dehydro amino acids in microcystin-LR and nodularin, two monocyclic peptide hepatotoxins from cyanobacteria (unpublished work) (Sivonen et al., 1992b).

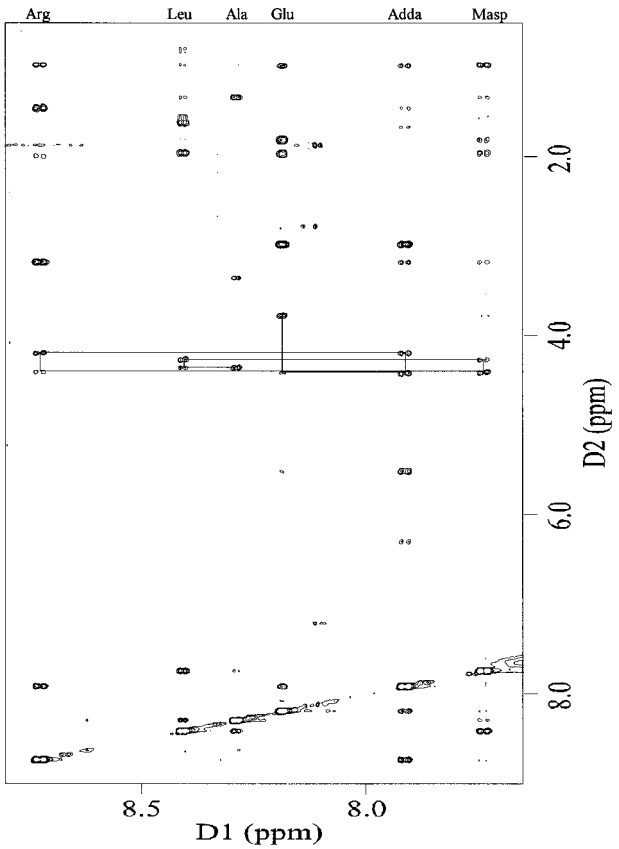

FIGURE 1: Fingerprint region of a NOESY spectrum of microcystin-LR recorded at 274 K in H_2O/D_2O at 600 MHz with a mixing time of 160 ms.

region of slow motion [$(\omega\tau_c)^2 \gg 1$] at these conditions. Hydrogen to deuterium exchange was also observed at 1 °C. Variable temperature experiments were conducted in the range from 1 to 41 °C. ROESY experiments were performed to examine dynamic processes such as possible conformational exchange. Proton relaxation times, T_1 and T_2, were measured using inversion−recovery and CPMG pulse sequences, respectively. All 2D data were zero-filled and then Fourier transformed to 2K × 1K data matrices. Chemical shifts were referenced to solvent signals, i.e., 2.50 ppm for DMSO/water and 5.01 ppm for water.

Extraction of Parameters for MD Calculations. All spin systems were identified from TOCSY and COSY/DQF-COSY spectra. The sequential assignment was derived from the connectivities in the NH/H−C(α) region of NOESY spectra. An expanded portion of a NOESY spectrum is shown in Figure 1. The chemical shifts of the nonexchanging protons are in good agreement with previous published assignment of microcystin-LR in deuterated methanol (CD_3-OD) (Harada et al., 1990a). Stereospecificity of geminal protons was concluded from ^3J coupling constants and NOE data.

2D NOE cross peak integration was carried out as a simple sum of points in a region with an optional subtraction of an average baseline per point. For every cross peak, a zoom box was adjusted to surround the region of integration. For more accurate determination of the volumes, surface fitting was applied with a convergence criterion of 0.01%. Interproton distances were generated from the 2D NOE cross peak integrals by using the program MARDIGRAS (Borgias & James, 1989, 1990). A complete 2D NOE relaxation matrix was set up using the geometry of a starting structure to account for all those interproton NOEs not available from the experimental data were used as starting models for the MARDIGRAS calculations. Three structures having substantially different conformations, i.e., structures with a pairwise rms deviation of more than 2 Å for backbone heavy atoms, were used. (An initial model of microcystin-LR with correct local geometry was subjected to unrestrained MD calculations at 1000 K to generate 10 different structures from which the three mutually most dissimilar structures were chosen.) Upper and lower bounds for interproton distances were obtained by comparing the results of the MARDIGRAS calculations while varying the starting models. All calculations were performed with a rotational correlation time, τ_c, of 2 ns in DMSO/H_2O and 1 ns in H_2O, respectively. These correlation times were derived from the relation between the experimental spin−lattice relaxation time (T_1) and the spin−spin relaxation time (T_2) (Suzuki et al., 1986). Simulations of DQF-COSY cross peaks, using the programs SPHINX and LINSHA (Widmer & Wütrich, 1986), were employed to allow an accurate determination of vicinal coupling constants from the spectrum recorded in DMSO/H_2O. This enabled determination of proton−proton coupling constants in the backbone as well as in the side chains. The *J*-doubling algorithm (McIntyre & Freeman, 1992) was used to extract coupling constants from spectrum recorded in H_2O. The obtained vicinal $^3J_{NH,H-C(\alpha)}$ coupling constants were corrected for the electronegativity effect of the C(α) substituents using the relation $^3J_{NH,H-C(\alpha)} = 1.09J_{obs}$ (Bystrow, 1976). Dihedral angles were calculated from the coupling constants by the Karplus equation (Bystrow, 1976) with the coefficients $A = 9.4$, $B = -1.1$, and $C = 0.4$ Hz for $^3J_{NH,H-C(\alpha)}$ and $A = 9.4$, $B = -1.4$, and $C = 1.6$ for $^3J_{H-C(\alpha),H-C(\beta)}$. For this study the $^3J_{NH,H-C(\alpha)}$ coupling constants were used as conformational constraints when greater than 8.0 Hz or smaller than 5.0 Hz: $^3J_{NH,H-C(\alpha)} > 8.0$ suggesting a ϕ between −80 and −125, $^3J_{NH,H-C(\alpha)} > 10.0$ suggesting a ϕ between −100 and −140 and $^3J_{NH,H-C(\alpha)} < 5.0$ Hz suggests ϕ between 155 and 195 (Glu). For Masp and Adda the dihedrals HA−CA−CB−HB were set to 55 ± 20 and 150 ± 30, respectively.

Restrained MD Calculations. The *ab initio* simulated annealing protocol (Nilges et al., 1988), described in the manual of the X-PLOR 3.0 program, was used to determine the three-dimensional structure of microcystin-LR. A set of 73 (97)[3] interproton distance restraints comprising 22 (26) interresidue and 51 (71) intraresidue distances and 8 (8) dihedral constraints were used for the calculation of the structure in DMSO/H_2O (H_2O/D_2O). Among the interresidue distances one originated from a NOE cross peak between Masp[3] and one of the β-protons in Glu[6] and in water also between Leu[2]HN and the same β-proton.

The starting structures for the SA calculations were varied to ascertain that the results represented a global energy minimum of the conformational space. Structures with different conformational properties were generated by exerting unrestrained MD at an elevated temperature (*vide supra*). The three most divergent of these structures, with a pairwise rms deviation of 2 Å or more for backbone heavy atoms, were used as a variable in the SA calculations. One hundred calculations using the SA protocol were carried out per template. Initial velocities were assigned from a Maxwellian distribution at 1000 K. The high temperature period

[3] Numbers in brackets refer to constraints obtained in aqueous solution.

Table 2: Root Mean Square Deviation from the Average Structure in Both Solvent Environments

	rmsd (Å)[a]	rmsd BB (Å)[a]
DMSO/water	1.36	0.15
water	1.32	0.18

[a] Calculated for heavy atoms.

consisted of 10 000 steps followed by 5000 steps for the cooling to 100 K. In subsequent refined SA calculations 7000 steps were used. The integration step was chosen to 0.003 ps. All SA calculations were followed by 300 steps of Powell's minimization algorithm. The number and size of distance-constraint violations and *R* factors have been exploited as a measure for the agreement between the model structure and NMR data.

Unrestrained MD Simulations. Unrestrained MD simulations of the molecule in water were performed by using the program CHARMm (Brooks et al., 1983). The structure with the lowest energy from restrained MD simulation was immersed in a box ($34.1 \times 27.9 \times 27.9$ Å^3) containing 863 water molecules. All water molecules closer than 2.8 Å to the solute molecule were removed. The entire system, comprised of the peptide and 795 water molecules, was subjected to free MD calculation with periodic boundary conditions. Initial velocities from a Maxwellian distribution were given at 98 K for all atoms. During the first picosecond the system was heated to 298 K and, after every 100 steps, the velocities were reassigned. The reassignment of the velocities was continued during the second picosecond if the temperature of the system was outside the desired temperature with more than ±10 K. Using the same criterion during the next 20 ps, the velocities were rescaled. The simulation after 22 ps was performed without any external perturbations. Integration of equations of motion was carried out using a step size of 1 fs. The lists for nonbonded and hydrogen bond interactions were updated after every 20 fs. The cut-off value of nonbonded interactions was set to 13 Å. Coordinates for all atoms in the system were recorded every 100 steps.

RESULTS AND DISCUSSION

Quality of the Structures. The spectra of microcystin-LR in both solvents contain only one set of signals at low temperature. Thus, there are no indications of exchange on the NMR time scale. Of the 300 calculated structures in each solvent, 228 structures in DMSO and 292 structures in water passed the acceptance test, which consisted of the ranges of bonds, angles, distance constraints, and dihedral constraints violations. The criteria for acceptance were as follows: rmsd for bonds, < 0.01 Å; rmsd for angles, < 2°; no NOE violations, > 0.3 Å; no constraint dihedral violations, > 5°.

The quality of the accepted structures has been analyzed using *R* factors, constraint violations, and rms deviations. The rmsd for all heavy atoms and backbone heavy atoms as compared with the average structure (Table 2) clearly shows that the cyclic backbone is very well defined. The major part of rmsd originates in the side chains.

The rmsd from the average structure as a function of atom number, shown in Figure 3, varies substantially within each calculation (DMSO/water and water, respectively). Bearing in mind that the backbone atoms contribute very little to the total value of rmsd, the significant variation of rmsd's calculated per residue originate largely from the different

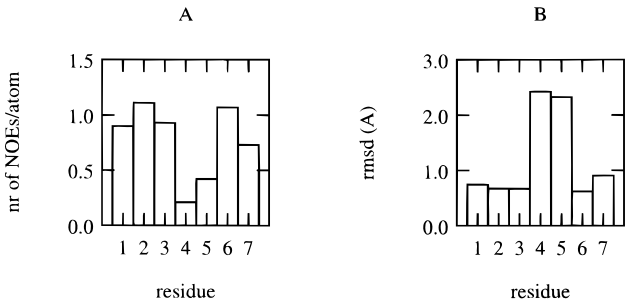

FIGURE 2: Correlation between the number of NOE constraints and the rmsd of the refined structures in DMSO/water. (A) The number of NOE constraints per atom and residue. All interresidue constraints are counted twice, once for each of the interacting residues. (B) Average rmsd from the average structure for the backbone atoms (N, C_α, C, and O in all residues, C_β in residue 3, 5, and 6, and C_γ in residue 6) as a function of residue number for the ensemble of 228 structures.

Table 3: Summary of Residual Constraint Violations[a]

	average number of distance constraint violations in	
range, *d* (Å)	DMSO/H_2O	H_2O/D_2O
$0.0 \le d < 0.5$	13.7	23.8
$0.05 \le d < 0.10$	18.5	11.8
$0.10 \le d < 0.15$	8.0	8.5
$0.15 \le d < 0.20$	1.0	3.9
$0.20 \le d < 0.25$	0.2	2.4
$0.25 \le d < 0.30$	0.2	2.8
$0.30 \le d$	0	0

[a] The force constant for distance contraints and dihedral constraints were 50 kcal mol^{-1} Å^{-2} and 50 kcal mol^{-1} rad^{-2}, respectively.

Table 4: Comparison of Sixth Root Residual Indices R_1^x of Starting Models and Resulting MD Structures

				DMSO/H_2O		H_2O/D_2O	
	start1[a]	start2[a]	start3[a]	all atoms	excluding Adda chain	all atoms	excluding Adda chain
R_1^x (intra)	0.085	0.151	0.156	0.082	0.076	0.074	0.070
R_1^x (inter)	0.118	0.257	0.219	0.078	0.079	0.073	0.075
R_1^x (tot)	0.094	0.180	0.173	0.081	0.077	0.074	0.072

[a] Calculated with $\tau_c = 1$ ns and NOE intensities observed in water.

constraint density in side chains (Figure 2A,B). In Table 3, the residual constraint violations are summarized. Most of the violations concern methyl groups.

The overall fit of theoretical and experimental NOE intensities is usually expressed by a residual index (Gochin & James, 1990)

$$R = \sum(|I_o| - |I_c|)/\sum I_o$$

The disadvantage of using this *R* factor is its tendency to favor strong cross peaks associated with short distances (<2.5 Å). Instead, a modified *R* factor, R_1^x, is preferred. R_1^x utilizes the sixth-root relationship between NOE intensities and appropriate distances (Thomas et al., 1991):

$$R_1^x = \sum(I_o^{1/6} - I_c^{1/6})/\sum I_o^{1/6}$$

where I_o and I_c are the intensities of observed and calculated NOE cross peaks. Table 4 lists residual indices R_1^x, calculated with the program CORMA (Borgias & James, 1989) for the starting models and the resulting structures. The calculations of the NOE intensities were based on the ensemble averaged relaxation rates over the number of

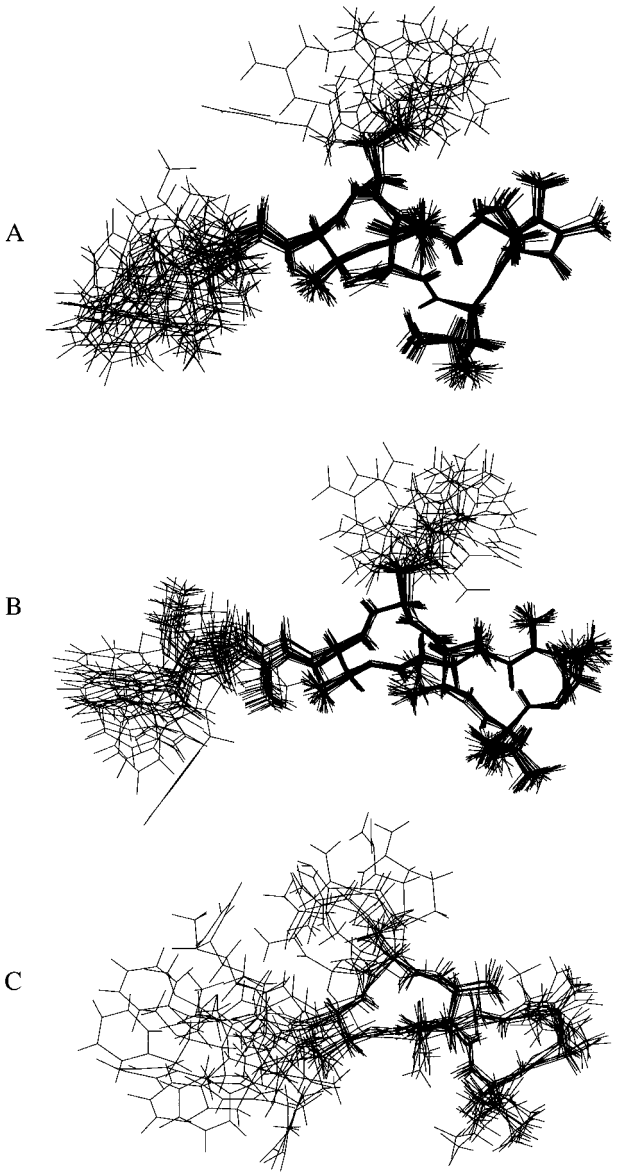

FIGURE 3: Superposition of 20 structures of microcystin-LR using randomly chosen structures among all accepted structures in DMSO/water (A) and in water (B). Panel C shows every 160 structures from 40 ps on, from the unrestrained MD-simulation.

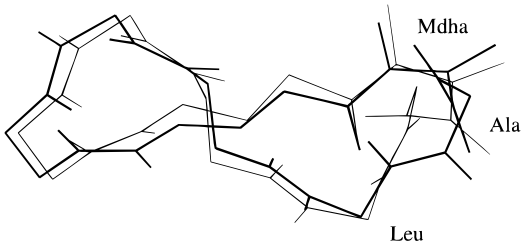

FIGURE 4: Superposition of the average structures (backbone atoms) from both solvents. The thick line represents the average structure where water is the solvent.

Table 5: Averages of Dihedral Angles from all Accepted Structures from Restrained MD

		angle (deg)		
residue	atoms	DMSO/H_2O	H_2O/D_2O	free MD
Ala	CA7-C7-N1-CA1	105 (7)[a]	149 (6)	178
	C7-N1-CA1-C1	116 (4)	77 (4)	95
	N1-CA1-C1-N2	11 (1)	22 (1)	−48
Leu	CA1-C1-N2-CA2	177 (3)	172 (2)	−179
	C1-N2-CA2-C2	−88 (8)	−111 (2)	−61
	N2-CA2-C2-N3	−22 (1)	−58 (1)	−44
Masp	CA2-C2-N3-CA3	117 (2)	−175 (9)	177
	C2-N3-CA3-CB3	−117 (3)	−126 (9)	−151
	N3-CA3-CB3-C3	−79 (2)	−75 (3)	−92
	CA3-CB3-C3-N4	−123 (13)	−118 (6)	−77
	CA3-CB3-C3-N4	−123 (13)	−118 (6)	−77
Arg	CB3-C3-N4-CA4	−179 (5)	−168 (4)	−177
	C3-N4-CA4-C4	−104 (13)	−115 (5)	−141, −89[b]
	N4-CA4-C4-N5	8 (23)	13 (21)	49, −40
Adda	CA4-C4-N5-CB5	171 (5)	166 (4)	170, −167[a]
	C4-N5-CB5-CA5	−95 (5)	−100 (4)	−152, −100[a]
	N5-CB5-CA5-C5	64 (1)	62 (4)	54
	CB5-CA5-C5-N6	−83 (5)	−108 (2)	−84
Glu	CA5-C5-N6-CA6	−167 (3)	170 (4)	−177
	C5-N6-CA6-CB6	141 (4)	−176 (5)	−176
	N6-CA6-CB6-CG6	154 (7)	168 (2)	170
	CA6-CB6-CG6-C6	161 (4)	165 (2)	−177
	CB6-CG6-C6-N7	155 (13)	160 (6)	174
Mdha	CG6-C6-N7-CA7	−144 (14)	−159 (11)	−176
	C6-N7-CA7-C7	36 (17)	19 (15)	−42
	N7-CA7-C7-N1	36 (22)	87 (10)	108

[a] Standard deviations are given in parentheses. [b] Two values are given when different conformations are observed in the free MD. The second value is the mean from 100 to 200 ps; the first is the mean for the rest of the time.

structures (228 for DMSO/H_2O and 292 for H_2O). As the NOE density per atom in the Adda residue is significantly lower in comparison to the other residues, the R_1^x factor calculated with and without inclusion of NOEs in the Adda side chain is shown.

Description of the Structures. The two families of solution structures of microcystin-LR are shown in Figure 3 (panels A and B). Superpositions of 20 structures, randomly chosen from all accepted structures in each solvent, are shown. The peptide ring is saddle-shaped in both solvents with carboxyl residues (Masp and Glu) on the sides (roughly in the "stirrup positions"). In both solvent systems, the Adda side chain is directed away from the cyclic backbone and also well defined in the proximity to the ring. No structures were found in which the Adda chain, which is essential for hepatotoxicity (Harada et al., 1990a,b), was bent into a position above the ring as has been suggested (Rudolph-Böhner et al., 1994).

Figure 4 depicts the superposition of the average structures of microcystin-LR in DMSO/water and water, respectively. The backbone segment Masp[3]-Arg[4]-Adda[5]-Glu[6] of the structure in the cryosolvent mixture is superimposed on the same backbone atoms in the water structure. The rmsd for backbone heavy atoms in this part of the structure is only 0.36 Å, and 0.65 Å for all heavy atoms in the backbone. The largest differences between the two structures can be seen in the segment containing the other three residues, i.e., Mdha[7], Ala[1], and Leu[2]. The conformational differences between the backbones in this region are due to changes of the backbone dihedrals in the vicinity of the amide bond between Mdha[7] and Ala[1] (see Table 5). As a result, the Ala[1]-NH in the two solvents points in different directions. It is interesting to see that the differences in the chemical structure between microcystins and nodularins are localized to the specific peptide portion in which the conformational difference between the two solution structures of microcystin-LR is obvious. Hence, we suggest for nodularin a very similar structure to microcystin-LR for the remaining homologous segment. These structural features are likely to be responsible for their similar biological properties.

The temperature dependence of the Masp[3]NH and the Adda[5]NH chemical shifts is minimal and very similar for both solvents (Table 6). This observation, as well as the presence of slow hydrogen to deuterium exchange rates

Table 6: Temperature Dependence of the Chemical Shifts, Given as $-\Delta\delta/\Delta T$ (ppb/°C)

	$-\Delta\delta/\Delta T$					
solvent	Ala[1]	Leu[2]	Masp[3]	Arg[4]	Adda[5]	Glu[6]
DMSO	11.6	6.0	0.0	7.2	0.7	2.6
water	6.4	4.9	−0.1	8.8	1.7	3.7

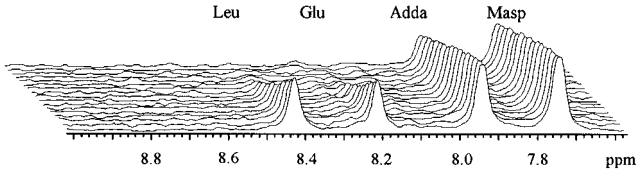

FIGURE 5: Exchange of amide protons to deuterium at 1 °C. Twenty minutes after the dissolution of the microcystin-LR in D_2O, the first spectrum was acquired. During that time, the NH of Arg and Ala had completely exchanged. The following three spectra were recorded with 20 min intervals, the next four with 30 min, and the last 10 at 1 h intervals. During the first 3 h, the LeuNH and GluNH exchanged entirely, while the intensity of the AddaNH was not reduced by more than 20% even after ~15 h. The NH of Masp remained essentially unaltered.

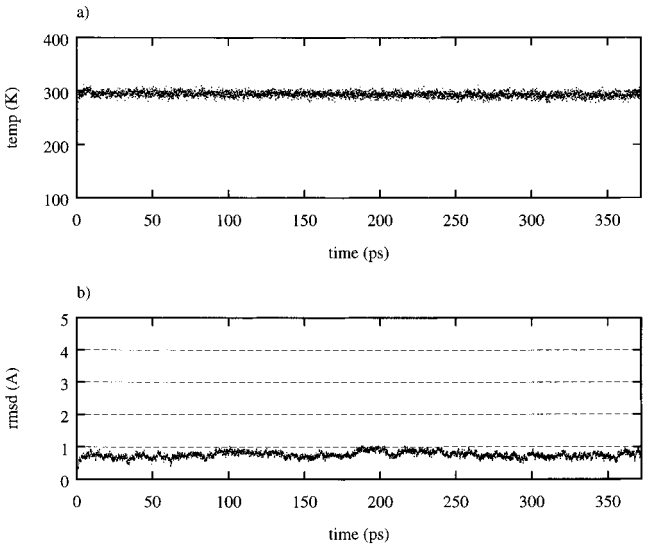

FIGURE 6: Convergence profiles of temperature (a) and rmsd from the starting structure (b) for 372 ps free MD on microcystin-LR including water.

(Figure 5), indicates that these protons are shielded from the solvent and that microcystin-LR has a well-defined structure. Using the cut-off criteria of 2.8 Å for the distance between donor and acceptor and 60° deviation of the hydrogen bond from linearity, we find only weak hydrogen bond interactions. In water, the NH of Leu[2] can pair with CO of Glu[6] while the distance between donor and acceptor is too long in DMSO/water. The difference in temperature dependence for the Leu[2]NH between the two solvents supports this. We also find that Glu[6]NH and Adda[5]NH can pair with COO^- of Masp[3] in both solvent environments. The Ala[1]NH and Arg[4]NH are directed outward and thereby exposed to the solvent. The difference in temperature dependence between the two solvents can be explained by the conformational divergence between the backbones in this region.

The restrained MD calculations result in one conformational family in each solvent that is clearly indicated by the low value of rmsd for the backbone heavy atoms. This is in contrast to results obtained by Böhner et al. (Rudolph-Böhner et al., 1994), who reported the existence of three conformational families in DMSO as a result of distance geometry calculations. These authors describe their family structures by defining a plane array of the peptide backbone of the amino acids Adda[5]-Glu[6]-Mdha[7]. Considering this segment as a flat part of the peptide backbone, our structures are in agreement with one of their families, with Arg protruding in one direction from this flat part and Leu-Masp on the opposite side. The saddle shape of the ring in our structures is in agreement with that of the DG calculated solution structures (aqueous) presented by Bagu et al. (1995) but differ from the results obtained by Lanaras et al. (1991) and Taylor et al. (1992), who predicted a planar ring using molecular modeling methods. Our calculated conformations of microcystin-LR are very similar to the crystal structure, where the toxin is complexed with protein phosphatase-1 (Goldberg et al., 1995). Interestingly, it appears that the DMSO/H_2O structure has the same conformation for Mdha, Ala, and Leu as compared to the phosphatase complex. Hence, the observed difference in solution structures represents the conformational change which microcystin-LR has to adopt upon binding to the enzyme in a water environment.

Results from Free MD Simulation and Comparison with Restrained MD Calculation. The disadvantage with restrained MD calculations is that possible flexibility within the molecule is neglected. In order to gain more insight into dynamic processes of microcystin-LR in solution, unrestrained MD simulations of the molecule in water were performed (Saulitis et al., 1992). Molecular dynamics calculation of microcystin-LR with explicit included water molecules was continued up to 372 ps. The temperature profile as a function of simulation time shown in Figure 6a, indicates a well-behaved and stable calculation. Additionally, the rmsd of the backbone atoms from the starting structure (Figure 6b) indicates a stable dynamic behavior of microcystin-LR during the whole simulation. The average value of the rmsd calculated for the total trajectory is 0.78 Å. Consequently, the 20 superimposed structures, chosen every 16 ps from the trajectory and shown in Figure 3C, appear to be very similar to the structures calculated using NMR constraints (Figure 3A,B). The greater flexibility of the Adda side chain during the free MD simulation is also obvious, while a conformation with the Adda side chain positioned over the ring, as suggested by Rudolpf-Böhner et al. (1994) was not observed.

Twenty-one out of the twenty-five torsion angles, defined along the backbone of microcystin-LR, show only small fluctuations at their starting values. This finding also strengthens the suggestion that microcystin-LR occurs in one major conformation only, at least on the subnanosecond time scale. The time development of the remaining four torsion angles, with changes over time, are shown in Figure 7. The average values of all backbone torsion angles are assembled under "free MD" in Table 5. Two values of the angles are given in the cases where the torsion angles clearly exist in two different states.

The interproton distance restraints generated from the 2D NOESY spectrum recorded in water were compared with their counterparts obtained as averages from free MD simulation. The difference, Δ, between the distance given by the latter and the closest value of the upper or the lower bound of corresponding restraint was calculated. Five distances for which Δ exceeds 0.5 Å are shown as profiles for the whole simulation time in Figure 8. Three of those,

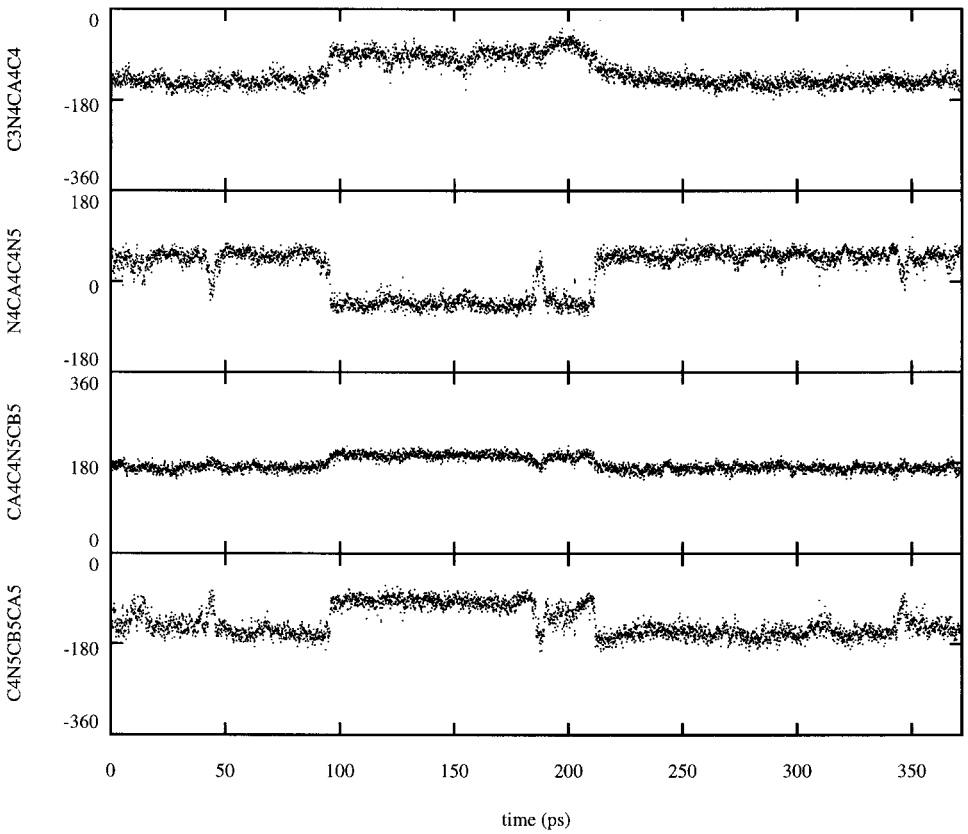

FIGURE 7: Evolution of the dihedral angles from the unrestrained MD simulation in water. Data are shown from 3720 coordinate data sets, sampled every 100 fs. For equilibration, 40 ps were used and, for analysis, 332 ps.

Leu^{2}HA−Leu^{2}HG, Adda^{5}H4−Adda^{5}HN, and Adda^{5}H5−Adda^{5}HB, involve side chain atoms, and therefore their deviations from the values predicted, using the NOESY spectrum, are reasonable in the light of their shorter rotational correlation times. The latter two distances, which are partially responsible for the alignment of the Adda side chain with the backbone of the peptide, occur in free MD simulation as two different states that are correlated in time with the observed rotation of the dihedral HB−CB−C4−H4 about the single bond C3−C4 in Adda (data not shown). The NOE data rules out that the conformation with the longer interproton distance could represent the solution structure. However, only a small population of the second conformation gave rise to the observed NOE intensity due to the inverse sixth power dependence on distance. Accordingly, the NOE intensity cannot distinguish between different population ratios. In contrast, experimental *J* coupling constants represent the time average of the existing conformations. The experimental coupling constant $^3J_{(\text{H-CB/H-C4})}$ (9 Hz) represents an average of the angles found in the MD trajectory. Consequently, both NOE and *J* coupling data are convertible with two local conformations in rapid exchange.

The fluctuation of the Glu^{6}HN−Adda^{5}HN distance correlates in time with the changes of the torsion angles C3−N4−CA4−C4, N4−CA4−C4−N5, CA4−C4−N5−CB5, and C4−N5−CB5−CA5 (see Figure 7) for which two different states were detected. The proton−proton coupling constant, corresponding to the dihedral C3−N4−CA4−C4, evaluated from the COSY spectrum, is 10.3 Hz, while the average value from the free MD is 4.8 Hz. However, in the range between 100 and 200 ps, the back-calculated mean value of this coupling constant is 10.7 Hz. Thus, the observed coupling constant indicates that the conformation found between 100 and 200 ps in MD is the predominant one. Moreover, the NOE data confirm the relevance of this suggestion since the observed NOE intensity gives the long distance found in this conformation, i.e., 2.5 Å rather than 2.1 Å.

Finally, the last distance with a large Δ value is the distance between Leu^{2}HN and Glu^{6}HB2. In free MD, the observed distance is in the range 3−6 Å. Thirteen percent (13%) of all saved structures have a distance shorter than 3.8 Å, which is the upper bound in the restrained MD calculations. Considering the relatively large error for long distances and the inverse sixth power dependence on distance, the experimental data are in agreement with the MD.

In general, the solution structures based on NMR measurements might represent time-averaged structures of rapidly exchanging conformations. The differences between the experimentally derived and the dihedral angles from the trajectory of the peptide in the free MD simulation are listed in Table 5. Relatively large deviations for angles in the Mdha part of the peptide can be seen. It might very well be so that the free MD simulation better describes the structure that does the SA calculation, as there are few constraints where Mdha is involved [no $^3J_{(\text{NH,H}-\text{C}\alpha)}$ coupling constant and overlapping signals]. The Leu^2 side chain is well defined for both solvent structures of microcystin-LR. The $^3J_{(\text{H}-\text{C}\alpha,\text{H}-\text{C}\beta)}$ coupling constants can reveal conformations of the side chains (Montelione et al., 1989; Mierke & Kessler, 1993). If both $^3J_{\alpha\beta}$ coupling constants are smaller than 5 Hz, or if they differ by more than 5 Hz, the side chain has a well-defined conformation. For Leu^2, these coupling constants are 11.0 and 4.0 Hz, which clearly supports the results from the restrained MD calculations (11.3 and 5.0 Hz, respectively). The corresponding values obtained from the simulation in water are 9.3 and 6.7 Hz, respectively. The

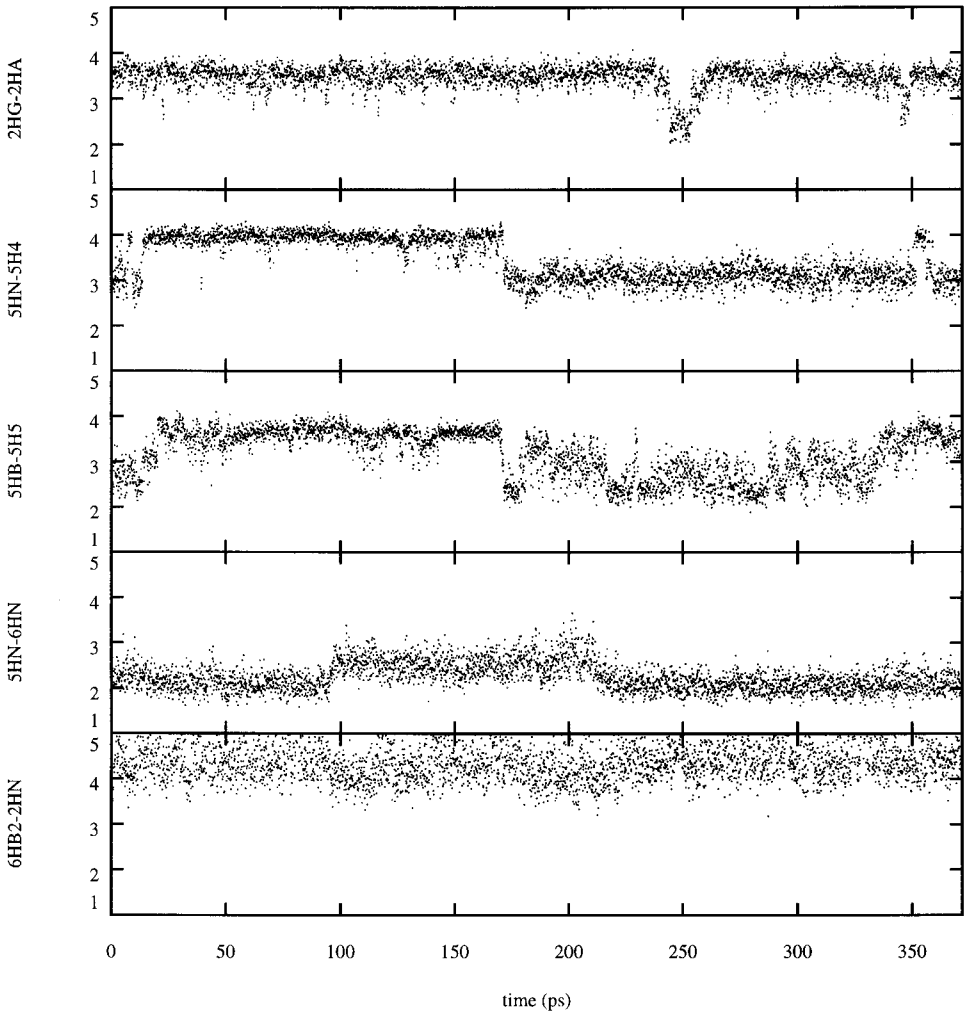

FIGURE 8: Evolution, during the simulation in water, of five distances, which deviate more than 0.5 Å from NMR data.

Table 7: Observed and Calculated $^3J_{HN-H\alpha}$ Coupling Constants

residue	$^3J_{HN-H\alpha}$ (Hz)		
	DMSO/H_2O[a]	H_2O/D_2O[a]	free MD[b]
Ala	7.5 ± 1[c]	7.1 ± 0.5	7.6
Leu	7.6 ± 0.5	7.1 ± 0.5	8.3
Masp	10.9 ± 0.5	10.7 ± 0.5	9.0
Arg	12.0 ± 0.5	10.6 ± 0.5	4.8 (2.9, 10.4)[d]
Adda	8.7 ± 1[c]	10.3 ± 0.5	10.5 (10.4,10.7)[d]
Glu	9.8 ± 0.5	4.0 ± 0.5	3.2

[a] Adjusted for electronegativity. [b] Calculated from water box data and then averaged. [c] From 1D spectrum. [d] Two values are given when different conformations are observed in the free MD. The second value in the parentheses is the mean from 100 to 200 ps; the first is the mean for the rest of the time.

Arg[4] side chain is highly disordered in both derived structural families. The mean values of the $^3J_{(H-C\alpha,H-C\beta)}$ coupling constants for this residue, calculated from SA structures, are 5.0 and 7.9 Hz. The result from the free simulation is 6.2 and 8.0 Hz, respectively.

The coupling constants for the Adda side chain (Table 8) indicate that the structure should be flexible in the remote part but better defined close to the backbone ring, since the coupling constant is 9 Hz between H-CB/H-C4 and H-C7/H-C8. The superimposed structures obtained from the restrained MD calculations (Figure 3A,B) show that the Adda side chain is well-defined for the part C4-C7, i.e., the entire conjugated system essential for the toxicity. The line widths also support this interpretation, as they are sharper for more distant protons.

Table 8: Some Observed and Calculated Vicinal Coupling Constants in DMSO/H_2O

residue	atoms	coupling constant (Hz)	
		observed	calculated[a]
Adda	H_2-H_3	11.0 ± 1.0	11.8
	H_3-H_4	9.0 ± 0.3	9.2[b]
	H_7-H_8	9.0 ± 1.0	9.5
	H_8-H_9	5.5 ± 0.5	5.9
	H_9-H_{10A}	6.0 ± 1.0	6.0
	H_9-H_{10B}	6.0 ± 1.0	6.0

[a] Vicinal coupling constants are calculated for each structure from Pachler's form of the Karplus equation where account is taken into the substituent effect (Pachler, 1972) and then averaged. [b] The MD calculations were performed without using dihedral constraints in the Adda chain.

Conclusions. The present results indicate that microcystin-LR in solution essentially adopts a single backbone conformation. The backbone of the peptide is saddle shaped with the flat-like part including the residues Adda[5]-Glu[6]-Mdha[7]. The side chains of Arg[4] and the remote part of Adda[5] are quite flexible without any well-defined structure. No conformation with the Adda side chain positioned over the ring was observed as earlier suggested. These results are supported by the restrained MD calculation (simulated annealing) based on NMR measurements as well as free MD simulation of microcystin-LR in water.

Structural differences are found in the residues Mdha[7], Ala[1], and Leu[2] for the two solvents. The DMSO/water structure resembles more closely the structure of microcystin-

LR complexed with protein phosphatase-1. However, these structural differences appear not to affect the toxicity, since this part of the molecule is absent and substituted by 2-(*N*-methylamino)-2-butenoic acid (Mdhb) in the equally toxic cyclic pentapeptide nodularin.

ACKNOWLEDGMENT

The Swedish NMR-Centre is acknowledged for allowing Gull-Britt Trogen to use their Varian Unity-500 instrument. We thank Professors Astrid Gräslund and Torbjörn Drakenberg for valuable and stimulating discussions and Mr. Leonardo Hillkirk for extracting coupling constants from spectra recorded in DMSO/water.

SUPPORTING INFORMATION AVAILABLE

One table containing distances calculated from a NOESY spectrum in water and the corresponding average distances during the simulation without experimental constraints (3 pages). Ordering information is given on any current masthead page.

REFERENCES

Amodeo, P., Motta, A., Picone, D., Saviano, G., Tancredi, T., & Temussi, P. A. (1991) *J. Magn. Reson. 95*, 201−207.
Bagu, J. R., Sönnichsen, F. D., Williams, D., Andersen, R. J., Sykes, B. D., & Holmes, C. F. B. (1995) *Struct. Biol. 2*, 114−116.
Barford, D., & Keller, J. C. (1994) *J. Mol. Biol. 235*, 763−766.
Berg, K., Carmichael, W. W., Skulberg, O. M., Benestad, C., & Underdal, B. (1987) *Hydrobiologia 144*, 97−103.
Borgias, B. A., & James, T. L. (1989) *Methods Enzymol. 176*, 169−183.
Borgias, B. A., & James, T. L. (1990) *J. Magn. Reson. 87*, 475−487.
Botes, D. P., Tuinman, A. A., Wessels, P. L., Viljoen, C. C., Kruger, H., Williams, D. H., Santikarn, S., Smith, R. J., & Hammond, S. J. (1984) *J. Chem. Soc., Perkin Trans. 1*, 2311−2318.
Brooks, B. R., Bruccoleri, R. E., Olafson, B. D., States, D. J., Swaminathan, S., & Karplus, M. (1983) *J. Comput. Chem. 4*, 187−217.
Bystrow, V. F. (1976) *Prog. Nucl. Magn. Reson. Spectrosc. 10*, 41−81.
Carmichael, W. W. (1988a) in *Natural Toxins: Characterization, Pharmacology and Therapeutics* (Ownby, C. L., & Odell, G. V., Eds.) pp 3−16, Pergamon Press, London.
Carmichael, W. W., Eschedor, J. T., Patterson, G. M. L., & Moore, R. E. (1988b) *Appl. Environ. Microbiol. 54*, 2257−2263.
Codd, G. A., Bell, S. G., & Brooks W. P. (1989) *Water Sci. Technol. 21*, 1−13.
de Silva, E. D., Williams, D. E., Andersen, R. J., Klix, H., Holmes, C. F. B., & Allen, T. M. (1992) *Tetrahedron Lett. 33*, 1561−1564.
Eriksson, J. E., Toivola, D., Meriluoto, J. A. O., Karaki, H., Han, Y.-G., & Hartshorne, D. (1990) *Biochem. Biophys. Res. Commun. 173*, 1347−1353.
Fujiki, H., Suganama, M., Yoshizawa, S., Kanazawa, H., Sugimura, T., Manam, S., Kahn, S. M., Jiang, W., Hoshina, S., & Weinstein, I. B. (1989) *Mol. Carcinog. 2*, 184−189.
Fujiki, H., Matsushima, R., Yoshizawa, S., Suganama, M., Nishiwaki, S., Ishikawa, T., & Carmichael, W. W. (1991) *Proc. Am. Assoc. Cancer Res. 32*, 157.
Gochin, M., & James, T. L. (1990) *Biochemistry 29*, 11172−11180.
Goldberg, J., Huang, H., Kwon, Y., Greengard, P., Nairn, A. G., & Kuriyan, J. (1995) *Nature 376*, 745−753.
Harada, K.-I., Ogawa, K., Matsuura, K., Murata, H., Suzuki, M., Watanabe, M. F., Itzeno, Y., & Nakayama, N. (1990a) *Chem. Res. Toxicol. 3*, 473−481.
Harada, K.-I., Matsuura, K., Suzuki, M., Watanabe, M. F., Oishi, S., Dahlem, A. M., Beasley, V. R., & Carmichael, W. W. (1990b) *Toxicon 28*, 55−64.
Lanaras, T., Cook, C. M., Eriksson, J. E., Meriluoto, J. A. O., & Hotokka, M. (1991) *Toxicon 29*, 901−906.
MacKintosh, C., Beatlie, K. A., Klumpp, S., Cohen, P., & Codd, G. A. (1990) *FEBS Lett. 264*, 187−192.
Matsushima, R., Yoshizawa, S., Watanabe, M. F., Harada, K., Furusawa, M., Carmichael, W. W., & Fujiki, H. (1990) *Biochem. Biophys. Res. Commun. 171*, 867−874.
McIntyre, L., & Freeman, R. (1992) *J. Magn. Reson. 96*, 425−431.
Meriluoto, J. A. O., Sandström, A., Eriksson, J. E., Remaud, G., Craig, A. G., & Chattopadhyaya, J. (1989) *Toxicon 27*, 1021−1034.
Mierke, D. F., & Kessler, H. (1993) *Biopolymers 33*, 1003−1017.
Montelione, G. T., Winkler, M. E., Rauenbuhler, P., & Wagner, G. (1989) *J. Magn. Reson. 82*, 198−204.
Moorehad, G., MacKintosh, R. W., Morrice, N., Gallagher, T., & MacKintosh, C. (1994) *FEBS Lett. 356*, 46−50.
Motta, A., Picone, D., Tancredi, T., & Temussi, P. A. (1988) *Tetrahedron 44*, 975−990.
Namikoshi, M., Rinehart, K. L., Dahlem, A. M., Beasley, V. R., & Carmichael, W. W. (1989) *Tetrahedron Lett. 30*, 4349−4352.
Namikoshi, M., Rinehart, K. L., Sakai, R., Sivonen, K., & Carmichael, W. W. (1990) *J. Org. Chem. 55*, 6135−6139.
Namikoshi, M., Rinehart, K. L., Sakai, R., Slotts, R. R., Dahlem, A. M., & Beasley, V. R. (1992). *J. Org. Chem. 57*, 866−872.
Nilges, M., Gronenborn, A. M., Brünger, A. T., & Clore, G. M. (1988) *Protein Eng. 2*, 27−38.
Nishiwaki-Matsushima, R., Ohta, T., Nishiwaki, S., Suganuma, M., Kohyama, K., Ishikawa, T., Carmichael, W. W., & Fujiki, H. (1992) *J. Cancer Res. Clin. Oncol. 118*, 420−424.
Pachler, K. G. R. (1972) *J. Chem. Soc., Perkin Trans II*, 1936−1940.
Rinehart, K. L., Namikoshi, M., & Choi, B. W. (1994) *J. Appl. Phycol. 6*, 159−176.
Rudolpf-Böhner, S., Mierke, D. F., & Moroder, L. (1994) *FEBS Lett. 349*, 319−323.
Saulitis, J., Mierke, D. F., Byk, G., Gilon, C., & Kessler, H. (1992) *J. Am. Chem. Soc. 114*, 4818−4827.
Shichman, S. A., & Amey, R. L. (1971) *J. Phys. Chem. 75*, 98−102.
Sivonen, K., Kononen, K. L., Carmichael, W. W., Dahlem, A. M., Rinehart, K. L., Kiviranta, J., & Niemelä, S. I. (1989) *Appl. Environ. Microbiol. 55*, 1990−1996.
Sivonen, K., Namikoshi, M., Evans, W. R., Carmichael, W. W., Sun, F., Rouhainen, L., Luukkainen, R., & Rinehart, K. L. (1992a) *Appl. Environ. Microbiol. 58*, 2495−2500.
Sivonen, K., Namikoshi, M., Evans, W. R., Färdig, M., Carmichael, W. W., & Rinehart, K. L. (1992b) *Chem. Res. Toxicol. 5*, 464−469.
Suzuki, E., Pattabiraman, N., Zon, G., & James, T. L. (1986) *Biochemistry 25*, 6854−6865.
Taylor, C., Quinn, R. J., McCulloch, R., Nishiwaki-Matsushima, R., & Fujiki, H. (1992) *Bioorg. Med. Chem. Lett. 4*, 299−302.
Thomas, P. D., Basus, V. J., & James, T. L. (1991) *Proc. Natl. Acad. Sci. U.S.A. 88*, 1237−1241.
Toivola, D., Eriksson, J. E., & Brautigan, D. I. (1994) *FEBS Lett. 344*, 175−180.
Widmer, H., & Wütrich, K. (1986) *J. Magn. Reson. 70*, 270−279.

BI952368S